# Characterization of the Goubau line for testing beam diagnostic instruments

Jinst

Published by IOP Publishing for Sissa Medialab

Received: *September 30, 2017*
Accepted: *December 1, 2017*
Published: *December 12, 2017*

# Characterization of the Goubau line for testing beam diagnostic instruments

**S.Y. Kim,[a] F. Stulle,[b] C.K. Sung,[a] K.H. Yoo,[a] J. Seok,[a] K.J. Moon,[a] C.U. Choi,[a] Y. Chung,[c] G. Kim,[c] H.J. Woo,[c] J. Kwon,[d] I.G. Lee,[a] E.M. Choi[a] and M. Chung[a]**

[a] *Department of Physics, Ulsan National Institute of Science and Technology, Ulsan 44919, Korea*
[b] *Bergoz Instrumentation, Saint-Genis Pouilly 01630, France*
[c] *Rare Isotope Science Project, Institute for Basic Science, Daejeon 34047, Korea*
[d] *Korea University, Sejong 30019, Korea*

*E-mail:* mchung@unist.ac.kr

Abstract: One of the main characteristics of the Goubau line is that it supports a low-loss, non-radiated surface wave guided by a dielectric-coated metal wire. The dominant mode of the surface wave along the Goubau line is a $TM_{01}$ mode, which resembles the pattern of the electromagnetic fields induced in the metallic beam pipe when the charged particle beam passes through it. Therefore, the Goubau line can be used for the preliminary bench test and performance optimization of the beam diagnostic instruments without requiring charged particle beams from the accelerators. In this paper, we discuss the basic properties of the Goubau line for testing beam diagnostic instruments and present the initial test results for button-type beam position monitors (BPMs). The experimental results are consistent with the theoretical estimations, which indicates that Goubau line allows effective testing of beam diagnostic equipment.

Keywords: Beam-line instrumentation (beam position and profile monitors; beam-intensity monitors; bunch length monitors); Instrumentation for particle accelerators and storage rings - high energy (linear accelerators, synchrotrons); Instrumentation for particle accelerators and storage rings - low energy (linear accelerators, cyclotrons, electrostatic accelerators)



https://doi.org/10.1088/1748-0221/12/12/P12016

2017 JINST 12 P12016

## Contents



2017 JINST 12 P12016

## 1 Introduction

In the 19th century, a variety of transmission lines to propagate electromagnetic surface wave had been investigated to enhance the transmission performance [1–3]. In particular, Sommerfeld's single wire line [4] which is a cylindrical transmission line with finite conductivity, features an electromagnetic surface wave travelling with low loss along the long propagation length. In order to excite the surface wave on the wire and propagate it to the receiver, a surface wave launcher is needed. However, the radial surface wave component generated on the Sommerfeld line extends very far from the conductor. Therefore, the launcher for the surface wave excitation should be extremely large [5]. In order to overcome this disadvantage, Goubau [6] gave a solution for minimizing the field extension using a dielectric coating on the single conductor. Thus, the surface wave launcher became significantly smaller compared to the Sommerfeld line, and low-loss propagation over long distances was made possible [7, 8].

We note that one of the characteristic features of the surface wave generated along the Goubau line is that the dominant mode of the surface wave is $TM_{01}$ mode [9]. This mode is similar to the field pattern radiated by the charged particle beam inside the beam pipe. Hence, the electromagnetic surface wave travelling along the Goubau line can be used for emulating the signal from the charged particle beam. Therefore, it is expected that the Goubau line can be applied to test beam diagnostic instruments without requiring real particle beams from the accelerators. In addition, the operation frequency of the Goubau line is up to several GHz. In other words, the Goubau line can cover the GHz regime which cannot be easily achieved by simple single-wire setup due to impedance mismatching problems.

There have been several demonstrations for the usefulness of the Goubau line for testing beam diagnostic instruments. Characterizations of BPMs and current transformers have been performed by Thomas Jefferson National Accelerator Facility and Bergoz Instrumentation [10, 11] Also, a coupling impedance measurement has been reported in refs. [12, 13]. In addition to the

applications using the Goubau line, fundamental characteristics of the Goubau line have been investigated at Bergoz Instrumentation [14]. However, the detailed description of Goubau line characteristics for testing beam diagnostic instruments has been somewhat limited. In this paper, we present the fundamental characteristics of the Goubau line system such as S-parameters and signal generation along the Goubau line, and look into the possibility of its application for testing various beam diagnostic instruments such as beam position monitor, beam phase probe, and beam charge/current monitor.

## 2 Theoretical backgrounds

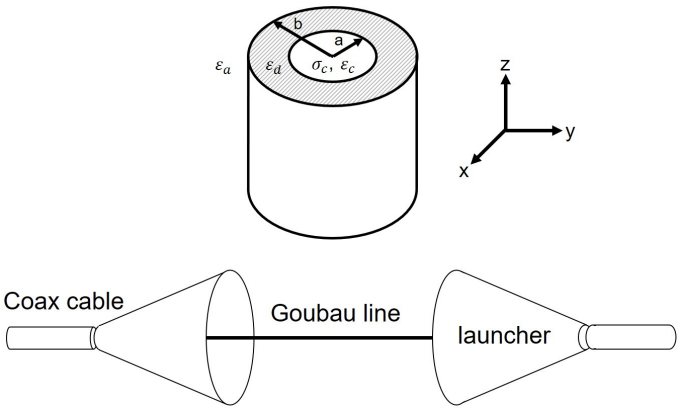


**Figure 1.** Schematic view of the Goubau line system including surface wave launchers and coaxial cable ports.

The Goubau line is made of a single dielectric coated conductor as shown in figure 1, where inner radius of the conductor and outer radius of the dielectric are denoted as $a$ and $b$, conductivity of the conductor wire is $\sigma_c$, and relative permittivities for each layer of air, dielectric, and conductor are $\epsilon_a$, $\epsilon_d$, and $\epsilon_c$, respectively. In the followings, Collin's description of the surface wave will be briefly summarized [15].

In order to get the surface wave solutions from the Maxwell's equations, some special conditions are needed. From Stratton [16], it is shown that the fundamental TE mode and higher modes along the wire are negligible because those modes rapidly decrease within short distances from the center of the wire. Therefore, we can use the assumption that there is an azimuthal symmetry (i.e., $\partial/\partial\theta \to 0$) [17]. In the cylindrical coordinates, electromagnetic field equations from the Maxwell's equations can be expressed as eqs. (2.1), where $\phi$ is a radial function, $k_0 = \omega\sqrt{\mu_0\epsilon_0}$, and $k_a^2 = k_0^2 - \beta^2$ in the air region $r > b$ and $k_a^2 = \epsilon_d k_0^2 - \beta^2$ in the dielectric region $a < r < b$, respectively.

$$E_z = \phi(r)e^{-j(\beta z-\omega t)}. \tag{2.1a}$$

$$E_r = -\frac{j\beta}{k_a^2}\frac{d\phi}{dr}e^{-j(\beta z-\omega t)}. \tag{2.1b}$$

$$H_\phi = -\frac{j\omega\epsilon}{k_a^2}\frac{d\phi}{dr}e^{-j(\beta z-\omega t)}. \tag{2.1c}$$

$$\frac{d^2\phi}{dr^2} + \frac{1}{r}\frac{d\phi}{dr} + k_a^2\phi = 0. \tag{2.1d}$$



2017 JINST 12 P12016

The general solutions of eq. (2.1) can be obtained by zeroth-order Bessel functions. In the air region $\phi$ can be solved by a modified Bessel function of the second kind. On the other hand, in the dielectric region, $\phi$ is a linear combination of Bessel functions of the first and second kinds.

$$\phi = BJ_0(hr) + CY_0(hr), \quad a < r < b. \tag{2.2a}$$

$$\phi = AK_0(pr), \qquad r > b. \tag{2.2b}$$

where $p = \sqrt{\beta^2 - k_0^2}$, $h = \sqrt{\epsilon_d k_0^2 - \beta^2}$, and $A$, $B$, and $C$ are some coefficients. Using boundary condition of $E_z = 0$ at $r = a$ to make the function $\phi$ to be zero, the coefficient $C$ is then

$$C = -\frac{BJ_0(ah)}{Y_0(ah)}. \tag{2.3}$$

Also from the boundary condition, $E_z/H_\phi$ must be continuous at the interface between the air and dielectric regions.

$$\left(\frac{E_z}{H_\phi}\right)_{\text{air}} = \left(\frac{E_z}{H_\phi}\right)_{\text{dielectric}}. \tag{2.4a}$$

$$\frac{K_1(pb)}{pK_0(pb)} = \frac{\epsilon_d}{h}\frac{J_0(ha)Y_1(hb) - J_1(hb)Y_0(ha)}{J_0(hb)Y_0(ha) - J_0(ha)Y_0(hb)}. \tag{2.4b}$$

Using the above eigenvalue equations (2.4a) and (2.4b), propagation constant $\beta$ can be calculated.

It is noted that the surface wave transmission power is determined by the input frequency, properties of the Goubau line, and launcher size [18]. In case of the Sommerfeld line which is a single conductor without dielectric coating, an extremely large launcher diameter is needed for high transmission efficiency (see figure 2). This is because the field extension in the radial direction is extremely large. However, for the case of the Goubau line, the launcher size is significantly reduced so that the surface wave can be excited more efficiently. We also note that from figure 2, reasonable frequency range to fabricate the surface wave launcher is the GHz domain. In the MHz domain, surface wave launcher is becoming too large even for Goubau lines.

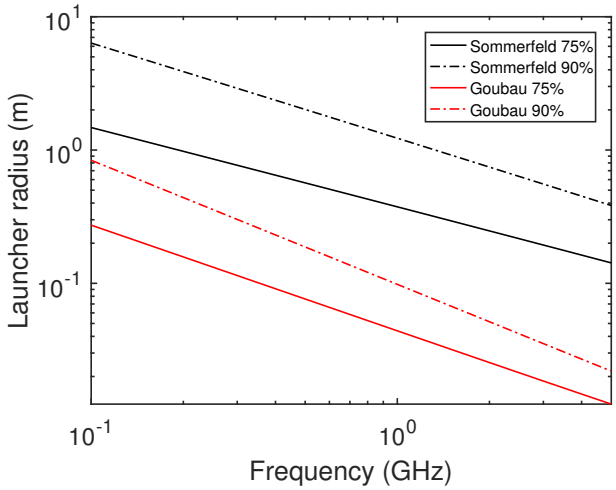


**Figure 2.** Calculated radius required to excite the surface wave with certain power transmission efficiency.

In addition to the Goubau line itself, which strictly speaking is just the single wire, there is a need for a surface wave launcher and a receiver. Launcher and receiver are made of a cone and a center conductor, which form a coaxial transmission liner taper. One of the most important features of the transmission line taper is to match the impedance between the signal source and the Goubau line system. Usually, the signal source will have 50 Ω impedance. The wave impedance of the Goubau line is determined by the wire properties and depends on frequency. Using an enamel coated wire and GHz frequencies the Goubau line impedance will be of the order of a few 100 Ω. The transmission line taper creates a smooth transition between the two impedances, minimizing reflections. In particular, our transmission line taper design is based on Klopfenstein-type [19] (known to be optimum [20]) and Hecken-type (known as near-optimum impedance matching section) [21] impedance matching sections. Reflection coefficients of the Klopfenstein-type and the Hecken-type tapers are given in eqs. (2.5).

$$\Gamma_K = \frac{1}{2}\ln\left(\frac{Z_2}{Z_1}\right)\frac{\cos\left[\sqrt{(\beta l)^2 - A^2}\right]}{\cosh(A)}. \tag{2.5a}$$

$$\Gamma_H = \frac{1}{2}\ln\left(\frac{Z_2}{Z_1}\right)\frac{B}{\sinh(B)}\frac{\sin\left[\sqrt{(\beta l)^2 - B^2}\right]}{\sqrt{(\beta l)^2 - B^2}}. \tag{2.5b}$$

Here, $\Gamma_K$ and $\Gamma_H$ are reflection coefficients of the Klopfenstein-type and the Hecken-type tapers, respectively. $Z_1$ is the coaxial cable impedance of 50 Ω, $Z_2$ is the coaxial cable impedance at the end of the launcher, $\beta$ is propagation constant of the Goubau line, $A$ and $B$ are Klopfenstein and Hecken parameters, and $l$ is the conductor length. In order to calculate the reflection coefficient of the transmission line taper, first the characteristic impedance $Z_2$ at the end of the surface wave launcher is determined by the radius of the cone and the radius of the inner conductor. For practical reasons, the diameter at the cone's wide end was chosen to be 200 mm. The cone follows a Gaussian shape to achieve a smooth transition. The diameter of the center conductor follows some numerically determined shape which creates a certain wave impedance evolution minimizing reflections. At the tip, the conductor diameter is 1 mm. Thus, the launcher transforms 50 Ω wave impedance to 317 Ω. Since the impedance of the Goubau line itself varies with the applied signal frequency and the wire characteristics (i.e., thickness of the dielectric coating, relative permittivity of the dielectric, and conductor radius), impedance mismatching cannot be fully avoided. In practice, it can only be minimized. With the given parameters, reflection and transmission coefficients of the Goubau line system can be estimated as the return loss and insertion loss which are S11, and S21 in the S-parameter notation.

In figure 3, it is depicted that the pattern of the return loss is periodic. Blue-colored graph (wave packet) of the S-parameter S11 indicates the characteristics of a single transmission line taper. Standing waves create signal minima at frequencies linked to the taper length. On the other hand, orange-colored graph shows the return loss along the whole Goubau line system including the receiver part. Distance between the launcher ends is 2 m, which means that the entire length of the Goubau line system is 2.82 m including the length of the launchers. For the calculation shown in figure 3, the repetition rate of signal minima is about 55 MHz. This means that the total length of the Goubau line system corresponds to half wavelength of this repetition rate [22].



2017 JINST 12 P12016

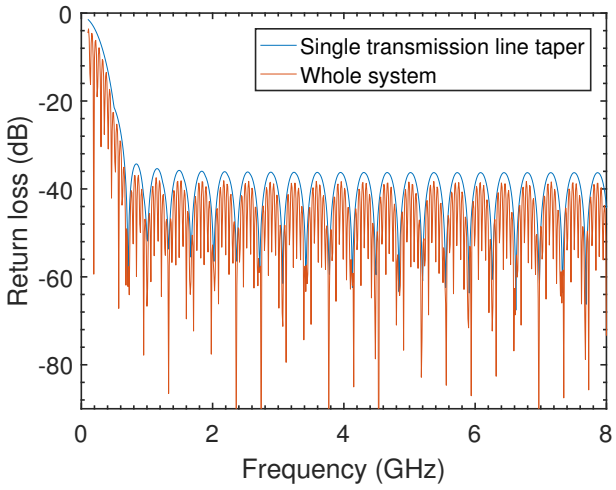


**Figure 3.** Theoretically calculated return loss of the Goubau line system.

## 3 Goubau line system and analysis of its fundamental characteristics

The Goubau line system manufactured by the Bergoz Instrumentation is shown in figure 4. The cones of the surface wave launchers depicted in figure 4(a) are mounted on the black acrylic holders for mechanical support and electrical isolation. Inside the cones, the center conductors are mounted [figure 4(b)]. To hold them firmly inside the cones, plastic lid structures are used [figure 4(d)]. At one end, center conductor and cone geometries allow connecting an N-type coaxial cable [figure 4(c)]. The Goubau line wire is then soldered to the launcher's center conductor. The radius of the bare copper wire is 0.35 mm and the radius with dielectric coating is 0.36 mm. Material of the dielectric coating is polyurethane. The setup is the same for the receiver on the right side in figure 4(a). The tension of the Goubau line wire should be kept constant to fix its position with respect to launcher, receiver and device under test. The S-parameter measurements presented below were performed using a Rohde&Schwarz ZNB-8 vector network analyzer.

First, the CST simulation [23] has been performed to check the basic characteristics of the Goubau line system, such as S-parameters and field patterns. Materials of the different parts have been set as follows; surface wave launcher and Goubau line conductor: copper, Goubau line dielectric coating: polyamide (dielectric constant is 3.5, which is similar to the polyurethane's dielectric constant that is in general 3.4), center conductor: brass. Distance between the ports is 2.82 m. Figures 5(a) and 5(b) are simulated E-fields along the Goubau line. Inside the surface wave launcher, longitudinal component of E-field can be seen as expected in ref. [24]. In the front view, generation of radial E-field and azimuthal H-field [figure 5(c)] along the Goubau line is clearly visible.

This field pattern is indeed $TM_{01}$ mode, which is the dominant mode of the Goubau line. From the E-field distribution illustrated in figure 6(a), it can be seen that the generated surface wave contains a standing wave structure along the Goubau line. When the input signal's wavelength is much longer than the length of the Goubau line system as in figure 6(b), then the surface wave cannot develop and will not propagate to the receiver end.



2017 JINST 12 P12016

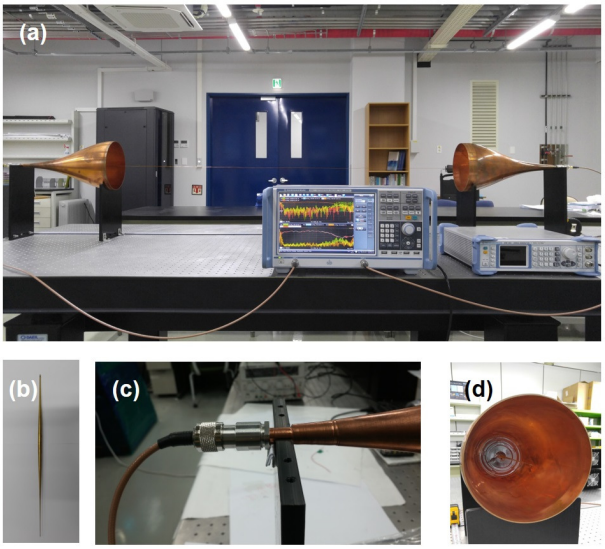


**Figure 4.** Goubau line system setup. (a): Goubau line system with surface wave launchers and a network analyzer. (b): center conductor (c): RF cable connection of the Goubau line system. (d): inside the surface wave launcher, a lid has been mounted to maintain the center position of the Goubau line.

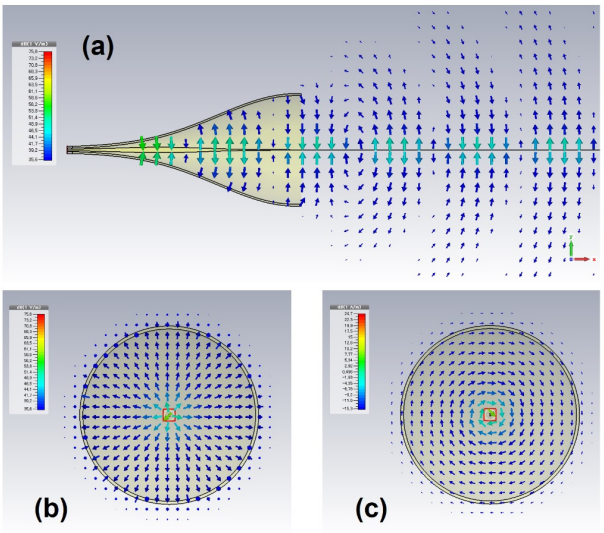


**Figure 5.** Electromagnetic field patterns at the input frequency of 1 GHz obtained from the CST simulation.

Figure 7 presents the S-parameters calculated by the CST simulation tool and measured experimentally in the frequency range from 100 MHz to 8 GHz. In order to compare the experimental results with the simulation data, we divide the frequency domain into three sections; 1) frequency range up to 600 MHz, 2) frequency range from 600 MHz to 5 GHz, and 3) frequency range from 5 to 8 GHz. In the first section, S11 is very high while S21 (insertion loss) is low compared to the GHz regime. As mentioned in section 1, transmission power is determined by physical radius of the surface wave launcher for a certain input frequency. In this frequency section, only 56.7%~ 70% of the input power can be transmitted, which corresponds to the insertion loss value of 4.932 dB



2017 JINST 12 P12016

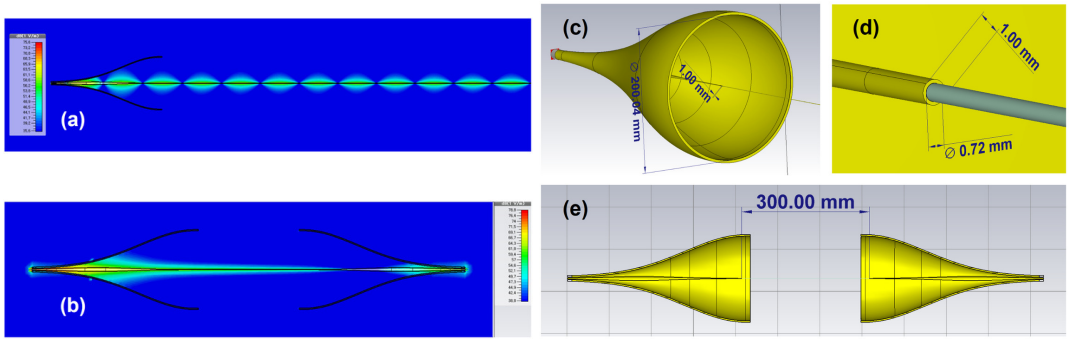


**Figure 6.** Simulated electromagnetic field patterns at the input frequency of 1 GHz with 2 m Goubau line (a) and 0.1 GHz with 0.3 m Goubau line (b), both of which are obtained by the CST simulations. Dimensions for the simulation of the Goubau line system are described in (c), (d), and (e). In (d), diameter of the Goubau line is 0.72 mm. In this case for the simulation, length of the Goubau line has been varied from 0.3 m to 2 m.

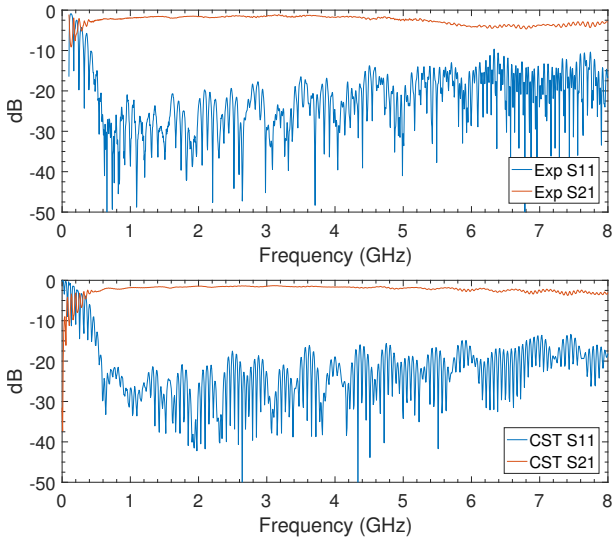


**Figure 7.** S-parameters measured from the experiments (top) and calculated by the CST simulation (bottom). The experimental data have been obtained with the Goubau line of 1.5 m, while the length used in the simulation is 2 m. Only the resonance patterns are slightly changed by use of different lengths.

to 3.107 dB. There is another loss term resulting from the wire and dielectric, however, it is rather small compared to the loss from the launcher (see ref. [6]).

In the second frequency section, transmission power is increasing with the frequency. Experimentally measured insertion loss and return loss in this section are typically 1.5 dB and 17 dB, respectively, which are consistent with the simulation results. These results can be converted into the Voltage Standing Wave Ratio (VSWR) of 1.329:1, which means 86% of the input power is transmitted to the receiving part.

On the other hand, in the third frequency section, insertion loss increases together with the return loss. It is due to the impedance of the Goubau line. The Goubau line impedance is changing as the increase of the input frequency, so there is an impedance mismatching between the transmission line taper and the Goubau line itself. This leads to an increase in the reflection



2017 JINST 12 P12016

coefficient, which in turn results in an increase in the insertion loss. By comparing the simulation results with the experimental data, we note that there appears some discrepancy for the insertion loss in this frequency section. This additional loss is likely due to the attenuation in the RF cable.

For the case of 2.82 m Goubau line system, frequency gap of the wave packet obtained by the simulation result is typically 354.6 MHz and that of the repetition of signal minima is 53.191 MHz, while the measured values are 318.75 MHz and 53.85 MHz, respectively. Resonance frequencies for different wire lengths are summarized in table 1. The measured frequencies are well matched to the calculated 1st harmonic resonance frequencies.

**Table 1.** Resonance frequencies for different wire lengths. The length of the two surface wave launchers (0.82 m) has been included for the calculation of the resonance frequencies.

| Goubau wire length (m) | 1st harmonic frequency (MHz) | Measured frequency (MHz) |
|---|---|---|
| 0.5 | 113.64 | 114.93 |
| 1.0 | 82.42 | 87.41 |
| 1.5 | 64.66 | 67.41 |
| 2.0 | 53.19 | 53.85 |
| 2.5 | 45.18 | 45.76 |

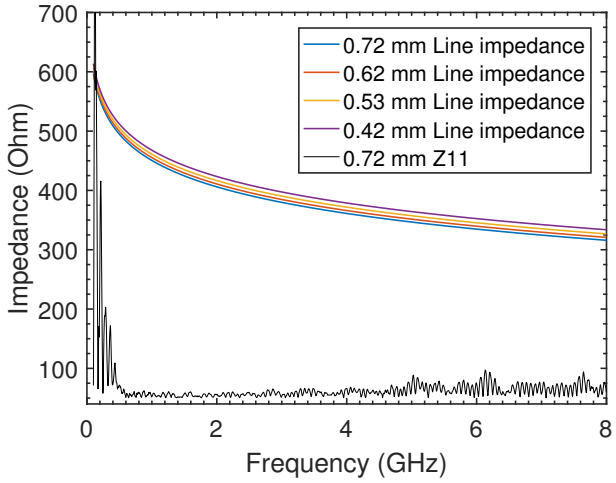


**Figure 8.** Calculated characteristic impedance of the Goubau line with varying thickness, and input impedance obtained by the S11 of the measurements.

Figure 8 presents the input impedance value obtained from S11, and calculated Goubau line impedance with varying thickness of the wire [25]. The impedance value obtained by S11 includes the reflection that occurs in the surface wave launcher, as well as the reflection caused by the transition at the end of the launcher with the impedance value of 317 Ohm. In the first frequency domain, the input impedance value is significantly higher than 50 Ω as expected. On the other hand, in the second frequency domain, the typical value converges to 50 Ω. However, as the frequency gradually increases to the frequency band above 5 GHz, the impedance value deviates from 50 Ω due to the impedance mismatch between the Goubau line and the 317 Ω at the end of the surface



2017 JINST 12 P12016

wave launcher. Indeed, if we examine closely the frequency band of 600 MHz or higher in figure 8, we can see that the S11 value gradually increases. This means that an impedance mismatch occurs as the characteristic impedance of the Goubau line changes with frequency.

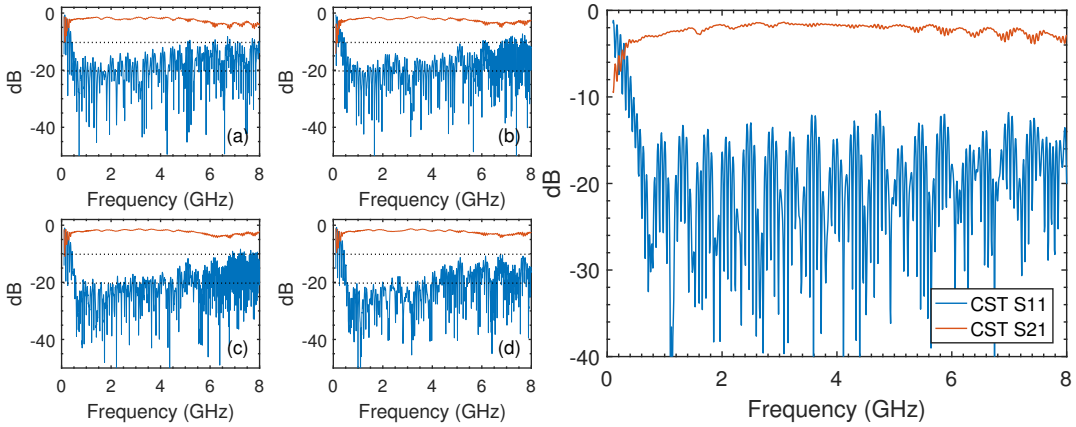


**Figure 9.** (left) S-parameters measured with different wire thicknesses. Overall diameter and dielectric thickness of the Goubau line wire are following: (a) 0.42 mm, 10 μm, (b) 0.53 mm, 15 μm, (c) 0.62 mm, 10 μm, (d) 0.72 mm, 10 μm. (right) S-parameters obtained by the CST simulation with 0.42 mm Goubau line wire.

Figure 9 shows the experimental result of measuring S-parameters with varying thickness of the Goubau line wire in 0.1 mm steps from 0.42 mm to 0.72 mm. It can be seen that the return loss increases as the thickness of the Goubau line becomes thinner. This tendency is mainly due to the discontinuity at the transition between the center conductor and the Goubau line. The center conductor in our setup is designed to be soldered to a wire of 0.9 mm diameter. Considering that the transmission line taper is designed to be continuous in terms of its shape for impedance matching, this discontinuity of the structure is resulting in an impedance mismatch. In our design, it contains a discontinuity since it has a feature of the Klopfenstein type transmission line taper. Using 0.9-mm diameter Goubau line wire will give optimum result. If the diameter of the Goubau line wire is larger or smaller than 0.9 mm diameter, the S-parameters will be worse as shown in figure 9. These experimental results are confirmed by CST simulations (figure 9 and figure 7 for comparison).

In addition, the relation between the S-parameters and the length of the Goubau line is shown in figure 10. The S-parameters have been measured while changing the length of the Goubau line in between the surface wave launchers. Somewhat different patterns of the S11 parameter above 6 GHz are due to the misalignment of the Goubau line with respect to the center position, and imperfection in the RF cable connection. If we focus on the nominal frequency range of 1 $\sim$ 3 GHz, the return loss is becoming larger when the length is decreasing as presented in figure 10(a). Meanwhile, as the length approaches 2 m, there is no change in the S-parameters except for the resonance frequency. This can be explained by wave development along the Goubau line. If the source frequency is 500 MHz, the period of the standing wave is nearly 30 cm, which is the half-wavelength of the source wave. When the length of the Goubau line system is less than the half-wavelength of the source wave, only a small fraction of the signal is transmitted. Also, considering the cases of 30 cm and 50 cm wire lengths, even though the source frequency is over 1 GHz (which corresponds to the



2017 JINST 12 P12016

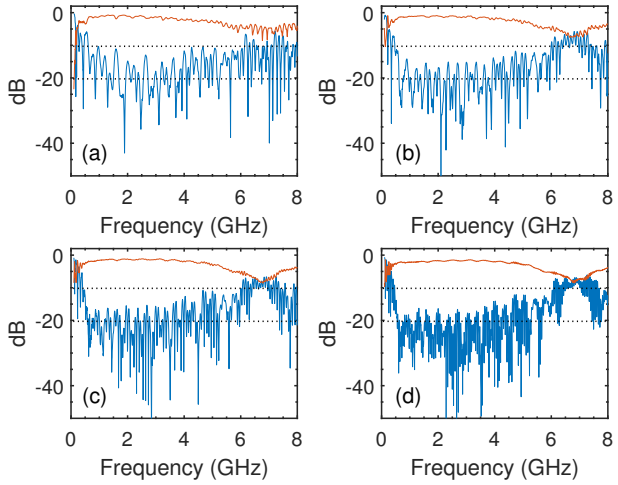


**Figure 10.** S-parameters measured with different wire lengths. Lengths of the Goubau line are following: (a) 0.3 m, (b) 0.5 m, (c) 1.0 m, (d) 2.0 m.

half-wavelength of 15 cm or shorter), the return loss is larger than the 2.0 m wire case. Therefore, in order to propagate the signal to the receiver part with a reasonably high transmission efficiency, the length of the Goubau line should be much longer than the half-wavelength of the source wave.

## 4 Signal analysis

To generate a continuous sine wave and a pulsed square wave along the Goubau line, a signal generator (SMB100A by Rohde&Schwarz) and a delay generator (DG645 of Stanford Research Systems) have been used. First, a sine wave scan has been performed to check the operation frequency. Figure 11 shows the measured voltage through the Goubau line and the ratio between the source and received signals.

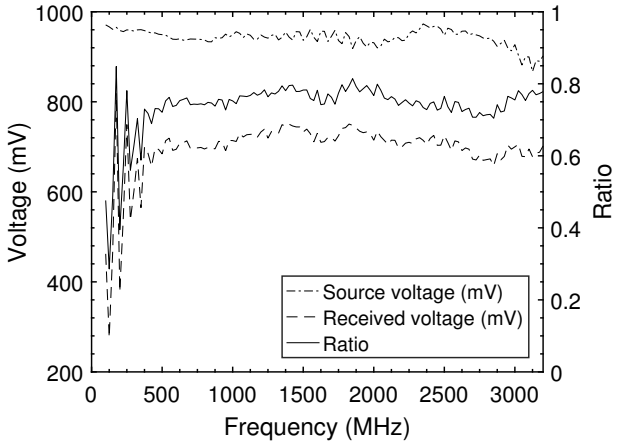


**Figure 11.** Amplitudes of the source and received sine wave signals, and the transmission ratio through the Goubau line.



2017 JINST 12 P12016

The source signal from the signal generator was measured directly from the oscilloscope, and the initial input voltage level is set to 1 V. Due to the cable attenuation, the typical value of the measured voltage amplitude is 950 mV. Also, the received voltage was measured by connecting the receiving port of the Goubau line to the oscilloscope while the source port was connected to the signal generator. In the MHz range, the amplitude of the received voltage is rather small due to the characteristics of the Goubau line. When the input frequency increases, the measured voltage amplitude is becoming larger. In the frequency range of 1 GHz to 3.2 GHz, ratios between the source and received signals are about 0.7, i.e., around 70% of the source signal can be transmitted in this frequency range.

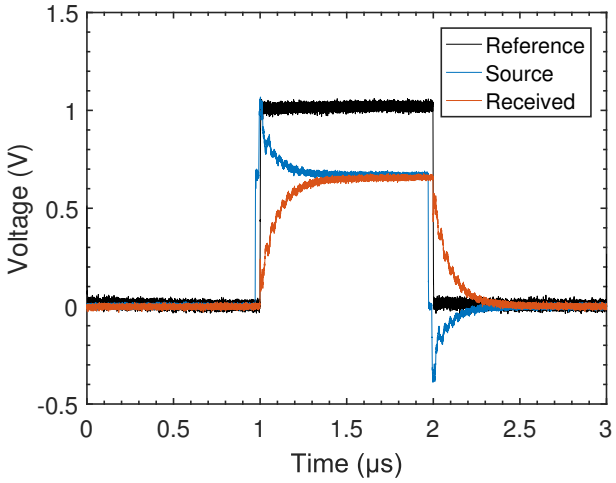


**Figure 12.** Experimental data for a square pulse signal with 1 μs pulse width. The shape of the source signal is distorted due to the reflection of the low frequency components.

Experiments with a pulsed signal have also been performed. As indicated in figure 12, a square pulse signal with 1 μs pulse width has been applied along the Goubau line with an input voltage level of 1 V. The source pulse signal is applied by using a BNC Tee adapter with connecting the source port of the Goubau line system. The rise and fall times of the initial pulse directly measured from the oscilloscope are 2.509 ns and 2.378 ns, respectively. Meanwhile, the rise and fall times observed from the signal through the Goubau line system are 184.633 ns and 186.887 ns. Also, one can see that there is an overshoot and ringing of the source signal. This can be explained in terms of the impedance matching issue.

Figure 13 shows the Fast Fourier Transformation (FFT) of the received pulse signal, and the S-parameters of the Goubau line system. According to figure 13, we note that the frequency characteristics of the received signal obtained by the FFT analysis match well to the S-parameters. For instance, frequencies of the local minimum in S11 are 31.35 MHz, 99.56 MHz, and 171.6 MHz. Due to the impedance mismatch, the power at certain frequency bands cannot be transmitted effectively. As a result, the rise and fall times of the pulse eventually increase. In order to reduce the rise and fall times of the sub-nanosecond pulse, it is essential to make an impedance matching at the frequency range of MF (medium frequency) and also VHF (very high frequency).

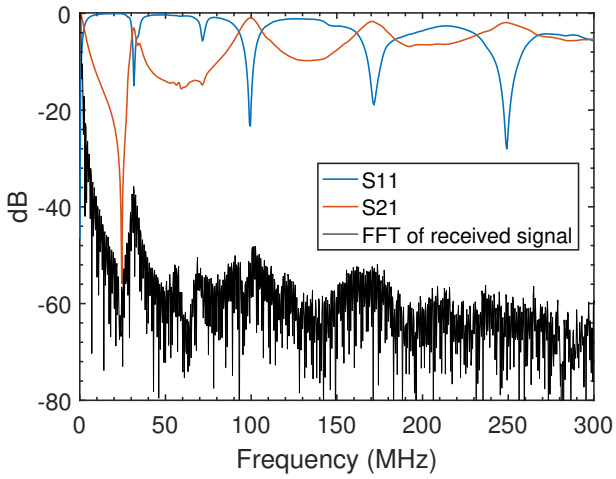


**Figure 13.** S-parameters of the Goubau line system and Fast Fourier Transformation (FFT) of the 1 μs-width square pulse signal.

## 5 Beam Position Monitor (BPM) test

The button-type Beam Position Monitors (BPMs) have been tested on the Goubau line as shown in figure 14.

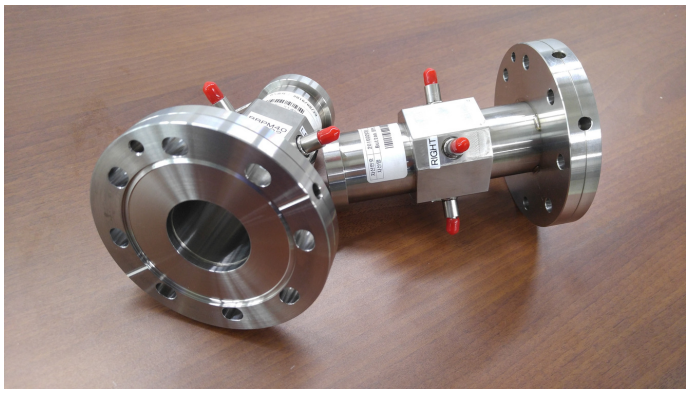

**Figure 14.** Button-type Beam Position Monitors (BPMs) developed for the Rare Isotope Science Project (RISP) in Korea.

The BPM was designed and manufactured for the Rare Isotope Science Project (RISP) in Korea, which is a heavy ion accelerator project to produce a wide variety of RI beams for nuclear physics experiments and other basic sciences. The fundamental frequency for the BPM is 81.25 MHz, and there are four electrode ports. The BPM detects the position and phase of the beam using the voltage signals measured through each port. Since the simple wire test bench does not have a proper impedance matching, we can test the BPM signal responses only up to 243.75 MHz, which is the third harmonic frequency of the system. On the other hand, the Goubau line system enables to measure the BPM signal responses at higher harmonic frequencies. Using one of the four electrodes, we measure the phase of the input signal detected by the BPMs installed along the Goubau line.



2017 JINST 12 P12016

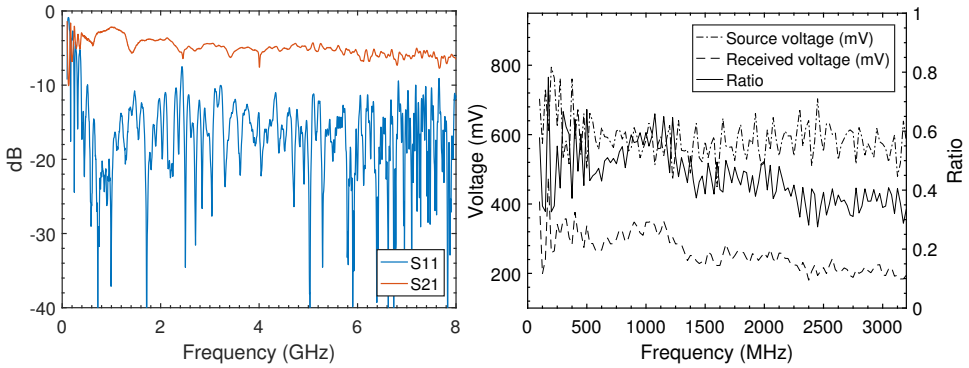


**Figure 15.** S-parameters (left), and voltage amplitudes and transmission ratio (right) for the Goubau line system with two BPMs. For the voltage signals, sine waves have been applied.

Figure 15 shows the S-parameters, source and received voltages, and their ratio, which are measured with two BPMs installed in the Goubau line. Due to the presence of the BPMs, the surface waves generated in the Goubau line are affected by the interference. The waveforms are distorted, and the transmission and reflection characteristics of the signals become somewhat inferior to the previous S-parameters which are measured without any BPMs (see figure 7 for comparison). The typical insertion loss in the GHz band is 5 dB and the return loss is 10 dB. Also, through figure 15, we note that the transmission ratio measured by using the signal generator and fast scope is approximately 40%∼ 50% at the GHz frequency region. Despite increasing return loss due to the BPMs, it is confirmed that still almost half of the voltage signals in the GHz band can propagate to the receiver end. It is noted that the source voltage in figure 15 is the value measured with the Goubau line and the signal generator connected using TEE adapter. This value is also consistent with the S-parameter S11 of the Goubau line.

Next, we performed phase measurements using the BPMs. Two BPMs were located at the center of the Goubau line system, and the separation between the BPMs is 0.243 m. An RF signal was applied at the frequency of an integer multiple of 81.25 MHz, and the phase difference was measured through the BPMs. In addition, the phase velocity of the surface wave was estimated based on the measured phase difference. The measured phase difference and the calculated phase velocity are shown in figure 16.

Due to the transmission and reflection characteristics of the Goubau line in a specific frequency band, it can be seen that the phase difference deviates much more from the expected value at MHz frequency band. However, as the input frequency increases, the phase difference approaches to the time range of 800 to 850 ps. Theoretical value of the phase velocity can be determined by $\omega/\beta$, where $\omega = 2\pi f$ and $\beta$ is the propagation constant in the Goubau line which is slightly larger than $k_0$. In the frequency range of 100 MHz to 8 GHz, the phase velocity obtained from the calculated $\beta$ is almost equal to the speed of light $c$. When the measured phase velocities are compared with the theoretically calculated phase velocities, the relative error is 3.75% at the input frequency of 812.5 MHz. Similarly, the relative errors at 975 MHz, 1137.5 MHz, 1300 MHz, and 1462.5 MHz are 0.13%, 6.22%, 3.69%, and 0.45%, respectively. For this preliminary test, the lack of dedicated motion stages and BPM mounts could bring about inaccurate alignment of the BPMs with respect to the center of the Goubau line, and might be a source of errors in the phase velocity estimations.

2017 JINST 12 P12016

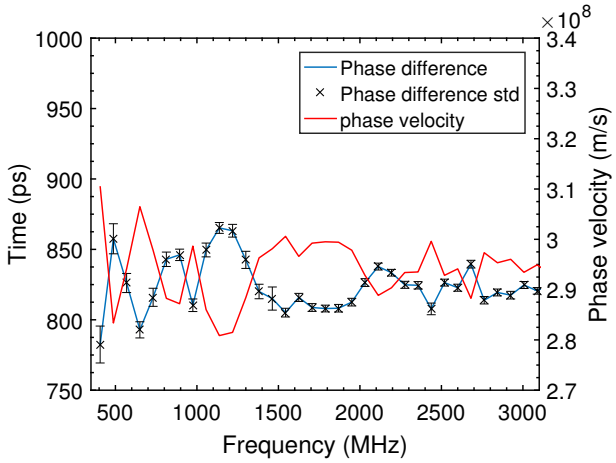


**Figure 16.** Plots of measured phase difference and reconstructed phase velocity as a function of input frequency.

This could be overcome in the future experiments by introducing a better alignment system. Such a system is also essential for calibrating position sensitivity of the BPM.

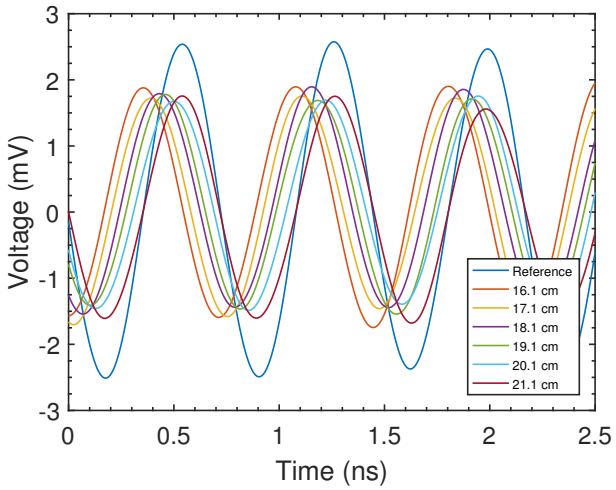


**Figure 17.** Measured sine wave signals with varying distance between BPMs.

Figure 17 illustrates sinusoidal waveforms measured by the BPMs. The input frequency is fixed at 1381.25 MHz which is the 17th harmonic frequency of BPM's fundamental operating frequency. One BPM is fixed at a certain position while the other BPM moves along the axis of the Goubau line, and the phase difference between them has been measured by comparing zero-crossing points of the waveforms. We manually adjusted the BPM distance from 0.161 to 0.211 m with 0.01 m step. The measured phase difference and phase velocity at each position are summarized in table 2. Although there are a few percent of relative errors, we demonstrate that the Goubau line enables precise phase delay measurements in the high frequency band of the BPM. More precise measurements will be made later with the installation of the BPM mounts and alignment system.



2017 JINST 12 P12016

**Table 2.** Measured phase difference and phase velocity with varying distance between two BPMs. Theoretically calculated phase velocity is $2.995 \times 10^8$ m/s.

| Distance (m) | Phase difference (ps) | Phase velocity (m/s) |
|---|---|---|
| 0.161 | 542.35 ± 3.950 | $2.969 \times 10^8$ |
| 0.171 | 573.36 ± 3.853 | $2.967 \times 10^8$ |
| 0.181 | 621.92 ± 4.060 | $2.910 \times 10^8$ |
| 0.191 | 659.63 ± 3.821 | $2.896 \times 10^8$ |
| 0.201 | 697.03 ± 3.720 | $2.884 \times 10^8$ |
| 0.211 | 740.81 ± 4.211 | $2.848 \times 10^8$ |

## 6 Conclusions and future work

Using a classical Goubau line with surface wave launchers, we performed basic characterization of the Goubau line system and applied it for the test of button-type BPMs. One of the important features of the Goubau line is a good impedance matching in the high frequency band, which enables the signal propagation in the GHz range without significant power loss. The phase responses of the BPM in the high frequency band have been measured precisely. It is expected that the installation of the BPM mounts and alignment system would further improve the precision of the phase measurements. In addition, it is planned to measure BPM responses with respect to the position of the Goubau line and to check the linearity of the position sensitivity. Through our experimental data, we confirmed that the surface waves generated by the Goubau line can emulate the electromagnetic fields emitted from the relativistic charged particle beams.

## Acknowledgments

This work was supported by the National Research Foundation of Korea (NRF) Grant funded by the Korean Government (MSIP) (Nos. NRF-2015R1D1A1A01061074, NRF-2016R1A5A1013277, and NRF-2017M7A1A1019375).

## References

[1] F. Harms, *Elektromagnetische Wellen an einem Draht mit isolierender zylindrischer Hülle*, *Ann. Phys. (Berl.)* **328** (1907) 44.

[2] J. Zenneck, *Über die Fortpflanzung ebener elektromagnetischer Wellen längs einer ebenen Leiterfläche und ihre Beziehung zur drahtlosen Telegraphie*, *Ann. Phys. (Berl.)* **328** (1907) 846.

[3] H.M. Barlow and A.L. Cullen, *Surface waves*, *Proceedings of the IEE-Part III: Radio and Communication Engineering* **100** (1953) 329.

[4] A. Sommerfeld, *Fortpflanzung electrodynamischer Wellen an einem zylindrischen Leiter*, *Ann. Phys. Chem.* **67** (1899) 233.

[5] G. Goubau, *Single-conductor surface-wave transmission lines*, *Proc. IRE* **39** (1951) 619.

[6] G. Goubau, *Surface waves and their application to transmission lines*, *J. Appl. Phys.* **21** (1950) 1119.

[7] C.E. Sharp and G. Goubau, *A UHF surface-wave transmission line*, *Proc. IRE* **41** (1953) 107.

[8] T. Roberts, *An experimental investigation of the single-wire transmission line*, *IEEE Trans. Antennas Propag.* **2** (1954) 46.

[9] F. Stulle, J. Bergoz and J. Musson, *Goubau line beam instrumentation testing, the benifits*, in proceedings of the *5th International Particle Accelerator Conference*, Dresden, Germany, June 2014, pp. 3462–3464,.

[10] S. Artinian, J. Bergoz, F. Stulle, V. Schlott and P. Pollet, *Goubau line and beam characterization of Turbo-ICT for Swissfel*, in proceedings of the *4th International Particle Accelerator Conference*, Shanghai, China, May 2013, pp. 476–478.

[11] J. Musson, K. Cole and S. Rubin, *Application of Goubau surface wave transmission line for improved bench testing of diagnostic beamline elements*, in proceedings of the *23rd Particle Accelerator Conference*, Vancouver, Canada, May 2009, pp. 4060–4062.

[12] M. Sangroula, R. Lindberg, R. Lill and X. Sun, *Impedance measurement of vacuum chamber components for the Advance Photon Source (APS) upgrade*, in proceedings of the *8th International Particle Accelerator Conference*, Copenhagen, Denmark, May 2017, pp. 3583–3586.

[13] F. Stulle, J. Bergoz and H.W. Glock, *Measurement of coupling impedances using a Goubau line*, in proceedings of *5th International Beam Instrumentation Conference*, Barcelona, Spain, September 2016, pp. 719–722.

[14] F. Stulle and J. Bergoz, *Surface wave for testing of beam instrumentation*, in proceedings of the *3rd International Particle Accelerator Conference*, New Orleans, U.S.A., May 2012, pp. 780–782.

[15] R.E. Collin, *Field theory of guided waves*, 2nd edition, McGraw-Hill, Inc. (1991), pp. 718–720.

[16] J.A. Stratton, *Electromagnetic theory*, McGraw-Hill, Inc. (1941), pp. 527–531.

[17] S.J. Orfanidis, *Electromagnetic waves and antennas*, Rutgers University New Brunswick (2002), pp. 509–525

[18] G. Goubau, *Surface wave transmission line*, PATENT Number US Patent 2,685,068, U.S.A. (1954).

[19] R.W. Klopfenstein, *A transmission line taper of improved design*, *Proc. IRE* **44** (1956) 31.

[20] R.E. Collin, *The optimum tapered transmission line matching section*, *Proc. IRE* **44** (1956) 539.

[21] R.P. Hecken, *A near-optimum matching section without discontinuities*, *IEEE Trans. Microwave Theory Tech.* **20** (2001) 734.

[22] F. Stulle and J. Bergoz, *The Goubau line - Surface waves for bench testing of beam instrumentation at high frequencies*, in proceedings of the *15th Beam Instrumentation Workshop*, Newport News, U.S.A., April 2012, pp. 146–148.

[23] Dassault Systèmes, *CST —Computer Simulation Technology*, (2017), http://www.cst.com.

[24] M. Friedman and F. Fernsler, *Low-loss RF transport over long distances*, *IEEE Trans. Microwave Theory Tech.* **49** (2001) 341.

[25] M. Gallant, *Goubau TM0 Wire Wave*, (2014), http://www.jensign.com/goubauwire/index.html.

2017 JINST 12 P12016